SCHOOL OF MATERIALS AND MINERAL RESOURCES ENGINEERING

UNIVERSITI SAINS MALAYSIA

CHARACTERIZATION OF LITHIUM VANADIUM OXIDE ANODE WITH AGAR BINDER IN AQUEOUS RECHARGEABLE LITHIUM ION BATTERIES

By

SOO KUAN LIM

Supervisor: Assoc. Prof Dr. Ahmad Azmin Bin Mohamad

Dissertation submitted in partial fulfilment

of the requirements for the degree of Bachelor of Engineering with Honours

(Materials Engineering)

Universiti Sains Malaysia

JUNE 2017

DECLARATION

I hereby declare that I have conducted, completed the research and written the dissertation entitled "**Characterization of Lithium Vanadium Oxide Anode with Agar Binder in Aqueous Rechargeable Lithium Ion Batteries**". I also declare that it has not been previously submitted for the award of any degree or diploma or other similar title of this for any other examining body or University.

Name of student : Soo Kuan Lim Signature:

Date: 20th June 2017

Witnessed by

Supervisor : Assoc. Prof. Dr. Ahmad Azmin Bin Mohamad Signature:

Date: 20th June 2017

ACKNOWLEDGEMENTS

To begin with, I would like to express my heartfelt gratitude and appreciation to my final year project supervisor, Associate Prof. Dr. Ahmad Azmin Mohamad for the valuable time and effort in guiding me all along in the course of the project and sharing his knowledge and experiences through presentations and advice.

Besides, I am very grateful and thankful to Ms. Nurul Nadia binti Mohd Zorkipli for she has guided me in full care in the handling of experimental and materials throughout the project. Furthermore, I would like to thank MOSTI for their financial support through the Science Fund Grant (03-01-05-SF0621).

Apart from that, I would like to convey my appreciation to all the technicians and supporting staffs especially Encik Azam, Encik Rashid, Encik Khairi and Encik Azrul of School of Materials and Mineral Resources Engineering for their kind assistance and cooperation provided in completing my final year project.

Finally, I take this opportunity to sincerely convey my appreciation to my family and friends for their relentless motivation, advice and support throughout the project. I have had a wonderful period discussing both theoretical and experimental ideas with friends and seniors alike which have indirectly contributed to the completion of this project.

TABLE OF CONTENTS

LIST OF TABLES

Page

LIST OF FIGURES

LIST OF ABBREVIATIONS

ARLB	Aqueous Rechargeable Lithium Batteries
CD	Charge-Discharge
CE	Counter Electrode
CV	Cyclic Voltammetry
EIS	Electrochemical Impedance Spectroscopy
FESEM	Field Emission Scanning Electron Microscope
ICSD	Inorganic Crystal Structure Database
OCP	Open Circuit Potential
R_{ct}	Charge Transfer Resistance
R_s	Electrolyte Resistance
RE	Reference Electrode
SCE	Saturated Calomel Electrode
WE	Working Electrode
XRD	X-ray Diffraction

LIST OF SYMBOLS

%	Percentage
o	Degree
Ω	Ohm
cm^2s^{-1}	Centimeter square per second
$mAhg^{-1}$	Mili-ampere hour per gram
Whkg-1	Watt hour per kilogram
^oC	Degree Celsius
$^oCmin^{-1}$	Degree Celcius per minute
A	Ampere
C	Current rate
cm	Centimeter
Mm	Micrometer
G	Gram
Hz	Hertz
V	Voltage
h	Hours

PENCIRIAN ANOD LITIUM VANADUM OKSIDA DENGAN PENGIKAT AGAR DALAM BATERI YANG BOLEH DICAS SEMULA DALAM ELEKTROLIT AKUES

ABSTRAK

Tujuan projek ini adalah untuk mengkaji kesan pengikat agar dalam anod litium vanadium oksida (LiV_3O_8) terhadap struktur, morfologi dan prestasi elektrokimia elektrod tersebut. Anod adalah diperbuat dengan menambah bahan aktif (LiV_3O_8), konduktor elektrik (grafene) dan pengikat (agar) dalam nisbah yang terperinci yang mana peratus agar dipelbagaikan. Elektrod bekerja tersebut dimampatkan dan dicirikan dalam sel separuh. Analisis struktur mengesahkan pengikat agar telah berjaya mengekalkan tetapan fasa LiV_3O_8 dan grafene sebelum kitaran. Manakala analisis morfologi membuktikan pengikat agar dapat mengelakkan ngah-laminasi bahan aktif dalam elektrod tersebut. Prestasi elektrokimia memperkukuh dapatan yang mana pencirian telah dijalankan dalam elektrolit 5 M $LiNO_3$. Keputusan kitaran voltammetri dengan kadar imbasan optimum iaitu 0.1 mV s^{-1} menunjukkan prestasi elektrod yang terbaik adalah elektrod yang mempunyai peratusan pengikat agar sebanyak 8%. Anod LiV_3O_8 ini juga mempunyai kebolehbalikan yang tinggi dan pekali penyebaran ion lithium yang tinggi, iaitu 1.315 x 10^{-6} dan 3.046 x 10^{-6} cm^2 s^{-1} bagi puncak anodik and kathodik masing-masing. Anod LiV_3O_8 juga menunjukkan permulaan kapasiti tertentu sebanyak 48 mAh g^{-1} di bawah kadar imbasan 0.1 Mv s^{-1}. Prestasi kitaran yang baik dicapai dengan 45 mAh g^{-1} (pengekalan kapasiti 93.75%) selepas kitran ke-10. Pengurangan kapasiti selepas itu disokong oleh penningkatan dalam rintangan pemindahan cas daripada analisis impedan. Kesan retakan pada permukaan anod LiV_3O_8 selepas kitaran dalam analisis morfologi menunjukkan perubahan isipadu anisotropik dalam kekisi parameter c semasa interkalasi/nyah-interkalasi ion litium.

CHARACTERIZATION OF LITHIUM VANADIUM OXIDE ANODE WITH AGAR BINDER IN AQUEOUS RECHARGEABLE LITHIUM ION BATTERIES

ABSTRACT

The purpose of this work is to study the effect of agar binder in lithium vanadium oxide (LiV_3O_8) anode on the structural, morphology and electrochemical performance of the electrode. The anode electrode is fabricated by adding the active material (LiV_3O_8), electrical conductor (graphene) and binder (agar) in a specified ratio with percentage of agar binder being varied. The working electrode is compacted and allowed to be characterized as a half-cell setting. The structural analysis indicate that the agar binder has successfully banded the phases of LiV_3O_8 and graphene together prior to cycling. The morphological analysis proven that the agar binder is able to prevent delamination of the active mass. The electrochemical performances further consolidate the findings where the characterization is done in 5 M $LiNO_3$ electrolyte. From cyclic voltammetry findings, with an optimized scan rate of 0.1 Mv s^{-1}, the best performing electrode is one with 8 wt% agar binder. The anode half-cell also had high reversibility and high coefficient diffusion of lithium ions at 1.315 x 10^{-6} and 3.046 x 10^{-6} cm^2 s^{-1} for anodic and cathodic peaks respectively. LiV_3O_8 anode demonstrated initial specific discharge capacity of 48 mAh g^{-1} under optimized scan rate 0.1 mV s^{-1}. A good cyclic performance with 45 mAh g^{-1} (capacity retention of 93.75%) at the 10th cycle. The capacity fading upon cycling was supported by increasing charge transfer resistance from the impedance analysis. However, cracks observed on the surface of LiV_3O_8 anode upon cycling in morphological analysis indicated anisotropic volume change in the lattice parameter c upon intercalation/de-intercalation of lithium ions.

CHAPTER 1

INTRODUCTION

1.1 Background

Secondary lithium ion batteries are modern power sources for portable electronic devices such as cellular phones, notebook computers and camcorders due to their high specific energy, high voltage, flexible and lightweight design and long shelf-life [1]. The demand of higher performance lithium ion batteries parallel with the compelling change in the renewable energy in the next decade. In lithium ion batteries, the main components are the electrodes and electrolyte; usually separated by a physical barrier packaged in a cell. The electrolyte can either be of organic substance or aqueous based electrolyte. Meanwhile, Aqueous Rechargeable Lithium Batteries (ARLBs) are systems based on water with its setup and charging-discharging mechanism is comparable to the traditional lithium ion rechargeable batteries [7].

For an anode material in particular, where lithium ions intercalate to the layered structure in the active material during charging. Nowadays, carbon based materials such as graphite are mainly more popular to be used as anode in ARLBs [4]. The prospects of metal oxide to be used as anode material is prevalent as recent reports [7] indicated that there are many types of metal oxide materials suitable to be used as anode such as vanadium oxides VO_3, Li-Mn spinels, nanostructured TiO_2, NASICON-type and pyrophosphate compounds.

During cycling, Li^+ are reversibly extracted and inserted into the framework of the lithium metal oxide structure by creating or annihilating vacancies within the

lithium planes. One possible way to achieve higher capacities is to design materials in which the metal-redox state can change structure, and allow the insertion of more than one Li^+ per transition metal. Such an approach is feasible with a few V-based oxides, where layered lithium vanadium oxide (LiV_3O_8) has high theoretical specific capacity of over 370 $mAhg^{-1}$ [2]. With fast lithium insertion / extraction kinetics ensured by the layered structure, LiV_3O_8 has been regarded as a promising anode material for lithium-ion batteries with high energy densities [3].

In anode fabrication process, a polymer binder is a material which is very important for binding the active materials and additive of the electrode together. The adhesive and chemical properties of the binder have a great impact on the performance of the battery, especially on the battery serviceability [4]. An optimal binder can prevent the active mass from baking away from the current collector as it reduces swelling in electrolyte. Such delaminating process of active mass leads to declining performance of the electrode during the process of charging-discharging, fast capacity fading and decreasing the battery serviceability [4]. For this reason, it is very important to select a binder which will reduce the delaminating of active mass.

1.2 Problem Statement

In order to produce aqueous rechargeable lithium ion batteries of higher performances, continuous developments in binder technology have been constantly improved to achieve the goal. Binder is crucial in maintaining the conductivity and battery performance. It has been reported that polyvinylidene fluoride (PVDF) is a traditional binder that exhibits excellent binding ability and meets the requirements of chemical and electrochemical stability [5]. It is important to note that PVDF is a type of

synthetic polymer added to the working electrode where the main phase is lithium vanadium oxide. In fact, most of the binders used in ARLB are of synthetic, polymer based. The pioneering work of Othman et al. [6] on zinc air electrode has shown that agar is another candidate that can be used for binders for the fabrication of porous anode electrodes. The possibility to use natural polymer binder such as bacto agar in ARLB open a wide potential leap in the research of this field. At the present moment, there remains a gap in study about the ability of the optimal ratio of agar binder to improve the electrochemical properties of ARLBs.

Commercial polymeric binders like PVDF are fluorinated polymers which can results in the deterioration of cycling performance of the batteries due to formation of stable LiF and double bonds (C=CF) upon reaction with Li metal or lithiated graphite (Li_xC_6) [5]. There exist problems like self-heating and thermal runway since the reaction of PVDF and Li is exothermal [8]. The stability of the resultant electrodes and the energy density of the electrode associated with agar binder has been the major barrier to the emergence of ARLB technologies.

There has not been previous research on LiV_3O_8 anode with agar binder to present on findings in electrochemical characterizations. Hence, there exists a compelling factor in investigating the interaction of agar binder, graphene and LiV_3O_8 as there could be non-desirable occurrences such as agglomeration when different ratio of agar binder is used.

1.3 Objectives

The objective of this study are:

i. To characterize the structural and morphological properties of pure LiV_3O_8

ii. To prepare the anode consisting of LiV_3O_8-graphene-agar at different ratios of agar binder

iii. To investigate the effect of agar binder on electrochemical properties of the LiV_3O_8-graphene-agar anode

1.4 Scope of Work

This chapter presents an introduction to the thesis with a brief explanation on the problems and the objectives of the present study. Chapter 2 will review on the introduction of lithium ion battery along with some basic concepts regarding the mechanism of the interaction of lithium ions Li^+. The interaction of Li^+ is discussed with relation to the structure of the layered vanadate oxide. Moving on, the interaction of agar binder in active material and graphene will also be reviewed. The electrochemical properties of LiV_3O_8 with binder in batteries such as cyclic voltammetry, electrochemical impedance spectroscopy, charge-discharge analysis and cyclic performance are also discussed.

Chapter 3 will explain on the methodologies used in this work, including the brief synthesis of LiV_3O_8 via sol-gel method, fabrication of the working electrode and the experimental setup of electrochemical characterization tests. The results of material characterization including structural and morphological analysis will be presented and discussed for further understanding. Along with that, results of the electrochemical characterization comprising of cyclic voltammetry (CV), electrochemical impedance spectroscopy (EIS), charge-discharge (CD) and cyclic performance (CP) are also discussed. Chapter 5 will summarize the whole thesis with conclusions and future works as recommendations.

CHAPTER 2

LITERATURE REVIEW

2.1 Introduction

This chapter provides a review of previous studies related to this research. Briefly, lithium ion batteries will be introduced in this chapter with its main components, working mechanism and common materials used to fabricate the battery. Focussing on aqueous rechargeable batteries, the working principles, prospects, science and engineering will be elaborated in detail with reference to previous work.

The properties of the active material, LiV_3O_8 will be studied and discussed together with the background on graphene and agar binder. Meanwhile, the components inside a lithium ion battery; in this case the anode will also be discussed briefly to understand the science and crystallography behind the working electrode. Moving forward, characterizations in terms of morphology and structure are examined in this chapter. Electrochemical characterization is one of the most important aspects in study with relations to lithium ion batteries hence will be subsequently reviewed in this chapter.

2.1.1 Lithium Ion Batteries

Lithium ion batteries as the name suggests; is a type of rechargeable battery in which the movement of lithium ions in and out of the working electrodes in producing electricity. To understand the background of its existence, the globalized era of industrial modernization in this century raised concerns on ecological needs and the importance of generating renewable energy sources. It is essential to promote new energy economy based on cheap and sustainable energy supply [1].

Coming into this context, secondary (rechargeable) battery can be discharged and recharged for a number of times in its lifespan of usage. Today, there is a variety of already stable rechargeable batteries which include lithium-ion, nickel-metal-hydride, and nickel-cadmium devices. However, lithium-based batteries, stood out among the conventional secondary batteries due to the fact that they have the highest energy densities, low self-discharge rate, wide operational temperature range and absence of memory effect as depicted in Table 2.1. This is mainly a result of electrochemical and physiochemical properties of Li. The application of Li hence is suitable to be used as power sources for electric vehicles with promising performances and flexibility in design.

Table 2.1: The comparison between various rechargeable batteries.

Cathode	**Anode**	**Electrolyte**	**Capacity retention (%) (per cycles)**	**Current density (mAg^{-1})**	**Capacity ($mAhg^{-1}$)**	**Ref.**
$LiFePO_4$	$LiTi_2(PO_4)_3$	Li_2SO_4 (1M)	90% (1000)	6.0 C	55	[57]
$LiFePO_4$ /C	VO_2	$LiNO_3$ (Saturated)	94% (50)	C/3	106	[58]
$LiFePO_4$ /C	LiV_3O_8	$LiNO_3$ (9M)	99% (100)	10.0 C	90	[59]
$LiFePO_4$	Activated Carbon	Li_2SO_4 (0.5M)	63% (10)	5.0 C	124	[60]
$LiFePO_4$	Activated Carbon	Li_2SO_4 (0.5M)	45%	20.0 C	58	[61]
$LiMn_2O_4$	VO_2	$LiNO_3$ (Saturated)	83% (42)	0.2 C	120	[62]
$LiMn_2O_4$	Activated Carbon	Li_2SO_4 (0.5M)	93% (10,000)	90.0 C	118	[63]
$LiMn_2O_4$	TiP_2O_7	$LiNO_3$ (5M)	85% (10)	0.2 C	42	[64]
$LiMn_2O_4$	Activated Carbon	Li_2SO_4 (0.5M)	99% (200)	4.5 C	110	[65]
$LiMn_2O_4$	Activated Carbon	Li_2SO_4 (0.5M)	94% (1200)	4.5 C	110	[66]
$LiMn_2O_4$	LiV_2O_5-Ppy	$LiNO_3$ (5M)	82% (60)	0.2 C	40	[67]
$LiCo_2O_2$	Ppy	Li_2SO_4 (Saturated)	63% (120)	0.1 C	104	[68]

2.1.1.1 Main Components of Lithium Ion Batteries:

A rechargeable lithium ion battery consists of a positive electrode (cathode), a negative electrode (anode) and a separator that splits both electrodes in the electrolyte, allowing the movement of ions instead of electrons. Certain lithium metal oxides can be used in both cathodes and anodes; however, some lithium metal oxides can only serve as anode alone or cathode alone. Figure 2.1 illustrates the basic working principles of lithium ion battery system. The Li^+ ion is hosted in a scaffold of cathode and anode electrodes as seen in Figure 2.1 (a) [11].

Meanwhile, when a battery discharges, chemical to electrical energy conversion occurs as Li^+ is extracted from the pentavalent structure of vanadium oxide, passes through the ionically conducting electrolyte with electron charge compensation taking place on the metal centre of the active cathode material. As for the electrons, they are to maintain a neutral electrochemical state when they travel through the external circuit from the anode to the cathode. The inverse process of charging the opposite reactions take place resulting in recharge ability.

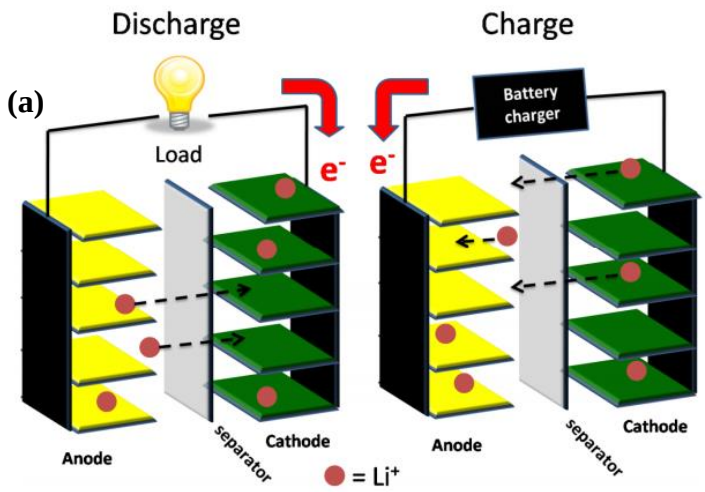

Figure 2.1 (a): Working principle of Li-ion battery de/insertion mechanism [11].

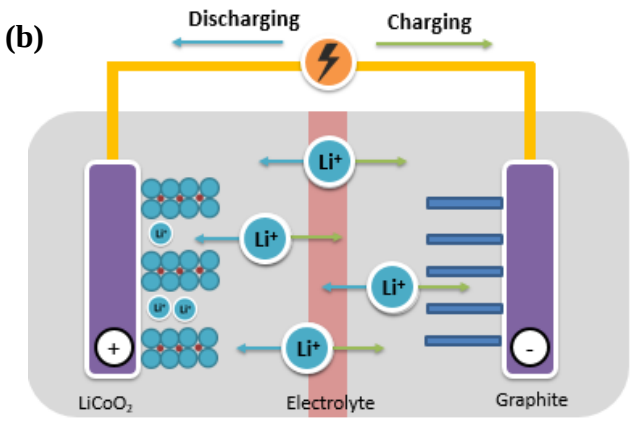

Figure 2.1 (b): Schematic representation of Li-ion battery de/insertion mechanism [11].

Charge compensation occurs on the cathode side as Li^+ and electrons shuttle back and forth between anode and cathode. There are changes in oxidation states of Co and V ions as charging and discharging occurs [12,13].

2.1.2 Aqueous Rechargeable Lithium Ion Batteries

In current commercial lithium batteries, the main concern which arises from the wide array of usage is on safety and reliability due to the usage of flammable organic liquid electrolytes in the battery system [1]. In this context, lithium-ion based batteries cannot be used in industrial scale storage of solar and wind energy and also the electric grid. Consequently, lead-acid rechargeable batteries are widely used for industries of heavier duty due to their good safety and low cost despite the negative contribute of environmental pollution. To replace this seriously ecologically depriving energy source, it is pivotal to now find substitute offering the same value proposition.

To begin with, recent reports have indicated that aqueous rechargeable batteries with lithium vanadium oxide as the anode, and other transition metal oxides such as $LiNi_{0.81}Co_{0.19}O_2$, $LiCoO_2$, $LiMn_2O_4$ and $LiNi/3Co/3Mn/3O_2$ as the cathode with

aqueous solutions of lithium salts as electrolyte exhibit a significant suitability as a renewable energy source [16-18]. By selecting appropriate transition metal oxides and electrolytes, electrochemical lithium intercalation reaction in aqueous electrolytes can be made possible [15].

However, in the early days, the most prominent problem of ARLBs is that they face a rapid capacity loss with cycling [19]. Considering the use of an aqueous electrolyte, the cell voltage is limited to the decomposition voltage of water (normally about 1.23V), which is lower than its closest competitor which uses organic electrolyte (>3V). The energy density of ARLBs decrease but still can be relatively efficient when compared to the likes of lead acid and Ni-Cd batteries [20]. The ARLBs are regarded as a promising power source since it is environmental friendly, relatively safe and deliver acceptable range of energy capacity.

A simple working mechanism on an aqueous rechargeable battery based on Lithium Cobalt Oxide, $LiCoO_2$ as the positive electrode and LiV_3O_8 as the negative electrode can be illustrated with the Figure 2.2 below. A layered of separation which contains the aqueous electrolyte can be clearly represented. The subsequent reactions taking place at each electrode respectively as indicated in the following equations [40]:

Positve electrode (Charging)

: $LiCoO_2 + LiV_3O_8 \rightarrow Li_{1-x}CoO_2 + Li_{1+x}V_3O_8$ (x < 1, at about 1.2 V) (2.3)

Negative electrode (Discharging)

: $Li_{1-x}CoO_2 + Li_{1+x}V_3O_8 \rightarrow LiCoO_2 + LiV_3O_8$ (x < 1, at about 0.9 V) (2.4)

The x value can be determined by complicated equilibrium equations or be referred and matched with ICSD data by running the sample through XRD analysis. It is also important to note that the negative electrode, termed the anode, can be replaced with any carbon based electrode which will not chemically participate in the chemical reaction and will only involve gas evolution in the mechanism [55].

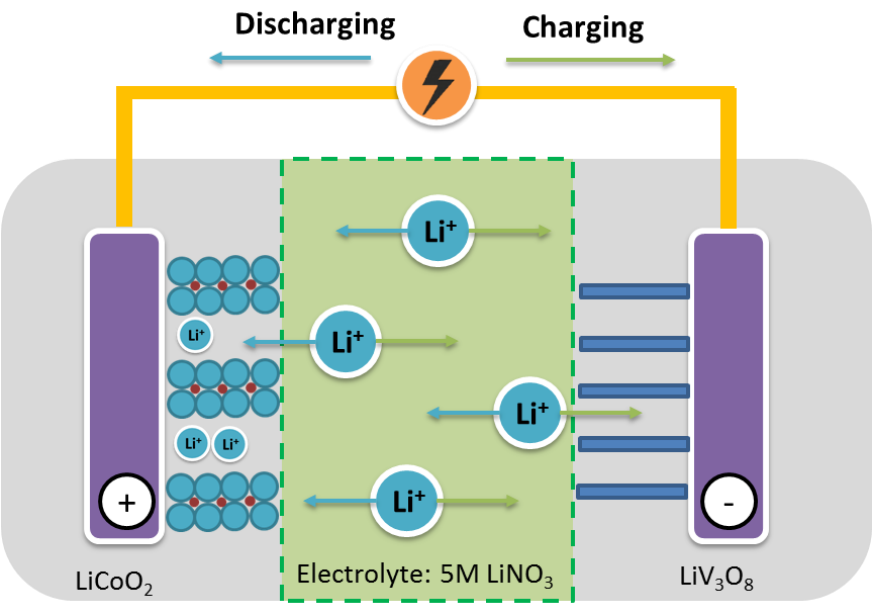

Figure 2.2: Schematic representation of ARLB mechanism [11].

2.1.2 Lithium Vanadium Oxide (LiV_3O_8) Anode

The three most important components in an ARLB is the cathode, anode and aqueous electrolyte. Here, the focus in on the anode material where it is considered as the negative electrode in which the electrons originally travel from this electrode to the positive electrode during the discharging process. Electrons will flow out of this electrode whilst current flows through it. It is important that the correct material should be used as a constituent of active material of this working electrode.

The LiV_3O_8 has a layered structure composed of two basic structural units, VO_6 octahedra and VO_5 distorted trigonal bipyramids [21]. The LiV_3O_8 is capable to function as an insertion electrode for rechargeable lithium batteries due to the fact that it can accommodate at least three additional Li^+ ions per formula unit. The lithium ions which occupy the octahedral sites linked to the V_3O_8 layer by strong ionic bonds, rendering a stable crystal structure of LiV_3O_8 during the charge-discharge process.

The mechanism in changes which happen in the structural level of intercalation of lithium can be indicated in the Figure 2.3 [22]. From the findings, it is proven that when lithium vanadium oxide electrode is used, there exists a reversible intercalation reaction. The readings from cyclic voltammetry support the evidence of this finding where there is a display of a stable reading when the cycles are increased. Also, the X-ray diffraction results revealed that the structural integrity of V_3O_8 layer is maintained after a series of cycling.

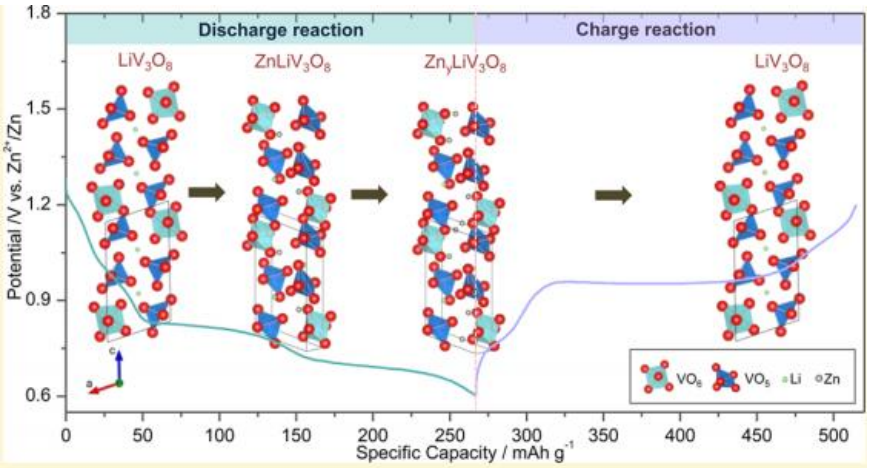

Figure 2.3: Changes in the structure of LiV_3O_8 during the electrochemical zinc intercalation in LiV_3O_8 [22].

Figure 2.4 (a) and (b) indicate the layered structural projections of LiV_3O_8. The work of Wadsley [23] after a series of structure refinement showed that the Li+ ions reside predominantly in an octahedral site, labelled Li (1) with site occupancy=1.0; the

excess lithium occupies one crystallographically independent tetrahedral site labelled Li (2) with site occupancy=0.10{5}. Hence, the refined composition is consistent with the chemically determined composition.

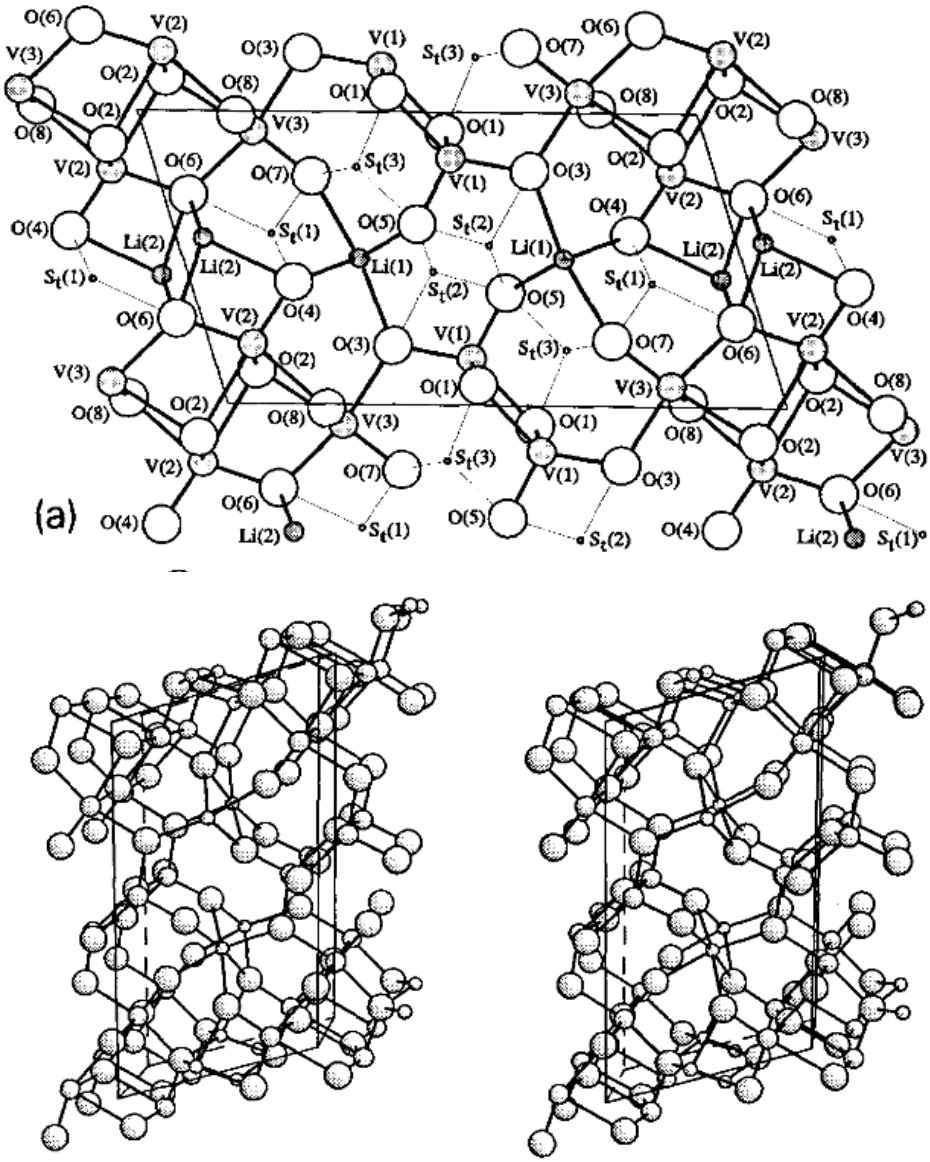

Figure 2.4 (a) indicate the atoms labelling and (b) represent the structural projections of LiV_3O_8 [23].

In order to study the intercalation mechanism, it is important to determine the potential of the intercalation compound and stability limit of water as a function of pH (ranging from pH 0-14) [9]. Pourbaix diagram is studied in relations the mechanism (Figure 2.5). An electrode with an intercalation potential in the range of 3-4 V vs Li^+/Li

is suitable as the cathode electrode for the ARLB (before the O_2 evolution). During discharge where reduction occurs, the Li^+ ions will be intercalated into the $Li_{l-x}Mn_2O_4$ (Figure 2.6). The $LiMn_2O_4$ immersed in 1 M LiOH undergoes the following reaction:

$$LilxMn_2O_4 + xLi^+ + xOH^- \rightarrow LiMn_2O_4 + (x/2)H_2O + (x/4)O_2 \quad (2.5)$$

This is expected based on the position of $Li_{l-x}Mn_2O_4$ relative to water at pH 14. Meanwhile, the where the intercalation of carbon placed in water will undergo the following reaction:

$$Li_xC_6 + xH_2O \rightarrow C_6 + xLi^+ + xOH^- + (x/2)H_2 \quad (2.6)$$

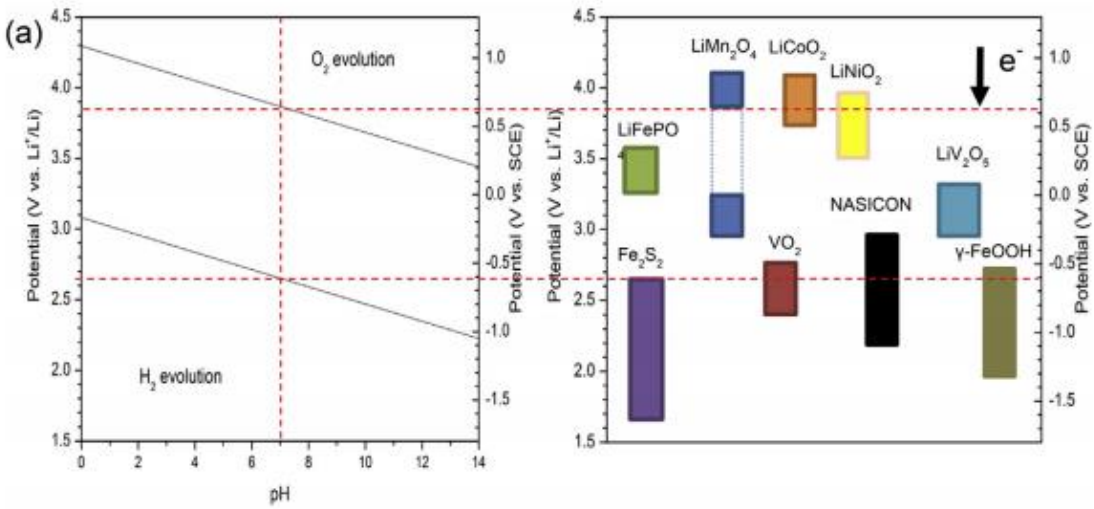

Figure 2.5: Stability potential window for intercalation/de-intercalation of Li ions for selected compound vs Li metal (left) and vs SCE (right) in aqueous solution [9].

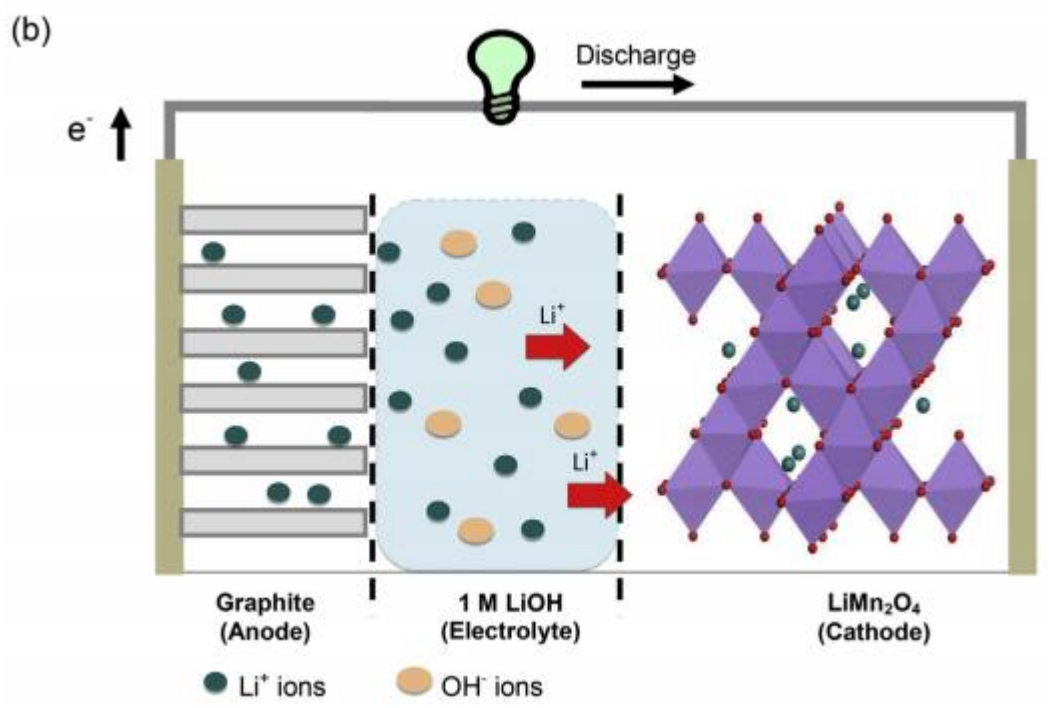

Figure 2.6: Schematic of cell configurations for the aqueous rechargeable lithium-ion battery [9].

2.2 Sol-gel Method

The layered structure of of LiV_3O_8 can be prepared by a few general synthesis methods. The two main synthesis methods include solid state reactions and sol-gel synthesis [24]. Moving forward, sol-gel route can produce LiV_3O_8 with homogeneous composition and higher capacity. With the addition of a chelating agent, the synthesis of LiV_3O_8 can be done at lower temperature (being at around 400 ^oC) as per compared to high temperature synthesis of solid state method. Kannan et al. [25] reported a comparison of the specific capacity of LiV_3O_8 prepared by solid state method and various conditions of preparation by solution dispersion method. A similar trend is obtained from the work Wang et al. [21]. It is apparent that the specific capacity of LiV_3O_8 prepared by solid state method is the lowest compared to the few variating parameters of solid dispersion method of preparation of LiV_3O_8.

Sol gel is a multi-step process involving both chemical and physical processes associated with hydrolysis, polymerization, gelation, condensation, drying and densification. To begin with, the process is started with mixing of metal alkoxides or salts in solvent to form sol at ambient or slightly elevated temperature [26]. The gelation of sol and the colloidal suspension of solid particles produce a gel consisting of rigid skeleton with pores made of the colloidal particles. To increase the homogeneity in the particle size distribution of LiV_3O_8, chelating agent is added [27]. Xerogel forms when the gel is heated to eliminate volatile organic components and excess water. Densification of xerogel is accomplished by calcination to obtain single phase LiV_3O_8 [28].

It has been confirmed that the flaky LiV_3O_8 prepared by a vapour diffusion controlled sol-gel method has a reversible capacity of 250 mAh g^{-1} and exhibited excellent capacity retention [29]. Comparing with other methods, Xu et al. [30] explored on hydrothermal reaction to synthesize LiV_3O_8 nanorods and the material had a reversible capacity of 302 mAh g^{-1} in a wider potential range of 1.8-4.0V. Sakunthala et al. [31] prepared LiV_3O_8 rods by a surfactant-assisted polymer precursor method, a discharge capacity of 206 mAh g^{-1} could be achieved in the potential range of 2.0–4.0V at a current density of 30 mAg^{-1}.

Liu et al. [32] first synthesized VO_2 nanorods as the vanadium precursor, and then employed solid-state reaction to fabricate LiV_3O_8 nanorods by adding $LiOH{\cdot}H_2O$. The LiV_3O_8 nanorods exhibited as high as 348 mAh g^{-1} initial discharge capacity at 20 mAg^{-1} in a wider potential window of 1.5–4.5V. Caballero and co-workers [33] synthesized LiV_3O_8 rods by using the precursors $VO(C_5H_8O_2)_2$ and Li(CH3–COO), and carried out the material as an electrode for aqueous rechargeable lithium batteries. Recently, a low-temperature thermal co-decomposition method was used for fabricating

a LiV_3O_8 nanorods [34], showing a particularly high discharge capacity of 320 mAh g^{-1} at a current density of 100 mAg^{-1} in the potential range of 1.5–4.0V.

2.2.1 Effect of calcination temperature

Higher calcination temperature leads to higher crystallinity due to more densification, resulting in a more well-defined layered structure of LiV_3O_8 as represented by Figure 2.7. Densification is maximised when sample is calcined at higher temperatures exceeding its recrystallization temperature. At this point, to further reduce internal energy, it can only be achieved by reducing the total area of grain boundary. In this process, grain growth occurs and this leads to a larger particle size. Since smaller particles have shorter diffusion path, this will enhance the intercalation and de-intercalation of Li^+, it is important that calcination temperature is sufficient to form pure LiV_3O_8 with layered octahedral or trigonal bipyramid layers with small particle size.

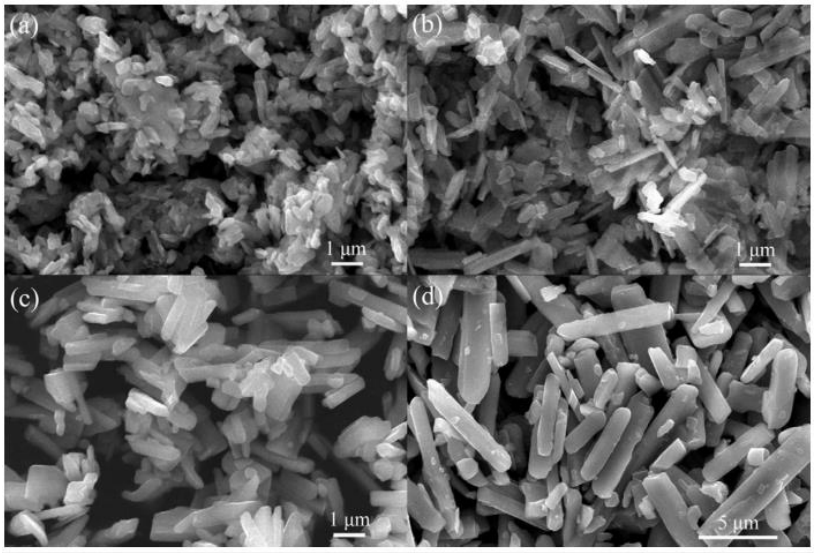

Figure 2.7: SEM images of the LiV_3O_8 samples synthesized at different temperatures: (a) 300 ºC; (b) 350 ºC; (c) 400 ºC; (d) 500 ºC [21].

2.3 Properties of Lithium Vanadium Oxide

2.3.1 Structural Properties

X-ray diffraction (XRD) is a common characterization technique to study the structural properties of LiV_3O_8, including its structure and phases. Since calcination temperature can affect the formation and electrochemical performance of LiV_3O_8, the effect of calcination temperature towards the structural properties of LiV_3O_8 will be reviewed.

Kohler et al. [1] reported that gamma phase, γ- LiV_3O_8 which show a high degree of crystallinity can be obtained by cooling a melt of a stoichiometric mixture of lithium and vanadium salts. The diffraction pattern of the starting as well as the resulting material is shown in Figure 2.9 (a,b) respectively. Subsequently, the LiV_3O_8 which has already high crystallinity can be further improved by annealing procedure at 550 ^oC for several hours in an oxygen atmosphere. The resulting reflexes which are more conspicuous in the corresponding X-ray pattern translates to an increased degree of crystallinity. At $2\theta=13^o$ is the diffraction at (100) plane indicating the layered structure of LiV_3O_8.

As mentioned earlier, these layers are made up of VO_6 octahedra and VO_5 trigonal bipyramids which are corner sharing with the octahera. The Li cations are to be intercalated between such layers. As particle size influence the electrochemical properties of electrode due to diffusion coefficient properties, it is important to study the effect of different type of particle size. Typically, for nanosheet lithium vanadium oxide, the XRD pattern observed has more significant peaks due to more controlled and smaller particle size which shows higher crystallinity (Figure 2.10) [49].

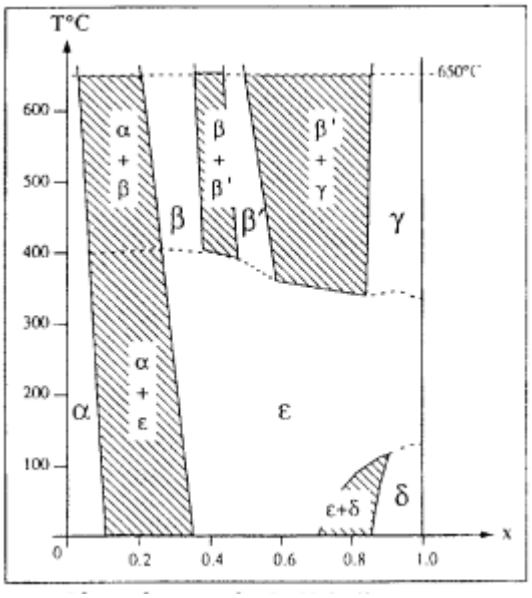

Figure 2.8: Stability diagram of $Li_xV_3O_8$ [14].

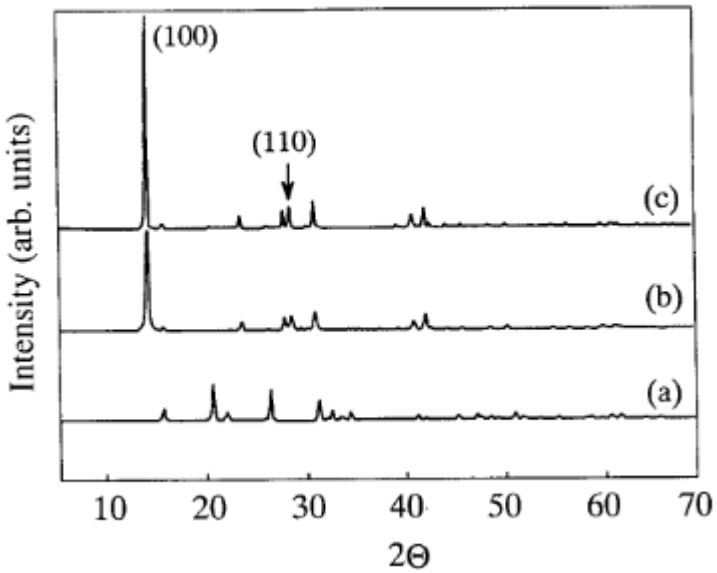

Figure 2.9: X-ray diffraction pattern of: (a) 2:3 mixture of LiOH and V_2O_5; (b) LiV_3O_8 as obtained from the melt; and (c) LiV_3O_8 after annealing at 550 ^oC for 8 h in oxygen atmosphere [1].

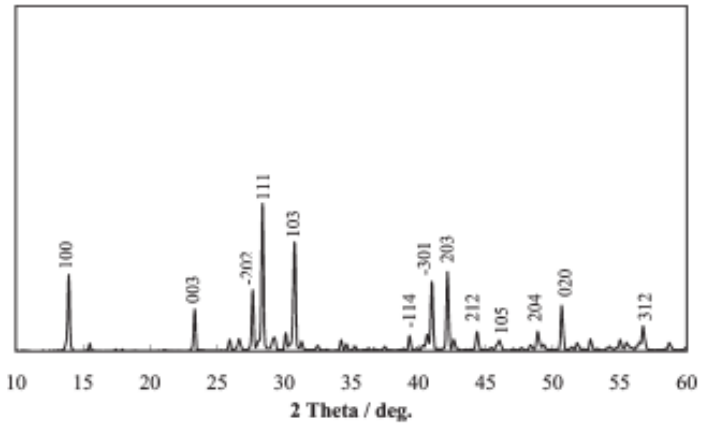

Figure 2.10: Typical X-ray diffraction pattern of LiV_3O_8 nanosheets [49].

In a separate experiment conducted by Kim et al. [36], to highlight the difference and similarities of $Li_{1.1}V_{0.9}O_2$ anode when it is discharged at 0.1C (charging rate). Accordingly, the crystallinity of the anode decreases as discharge reaction happened (Figure 2.11). When the cell is fully discharged, the structure of $Li_{1.1}V_{0.9}O_2$ changed into $Li_{2.1}V_{0.9}O_2$ corresponding to a decrease of oxidation number of vanadium from V^{+3} to V^{+2}. Also worth noting is that the peak (104) and the intensity of other main peaks in the XRD patterns were split into two peaks and decreased due to structural transformation during the lithium intercalation, respectively. As the cell was charged up to 1.5 V, the relative intensity of the peaks was almost recovered. This suggested that the phase stability of the $Li_{2.1}V_{0.9}O_2$ anode can be attributed from the homogenous distribution of the pure crystalline active material in the electrode.

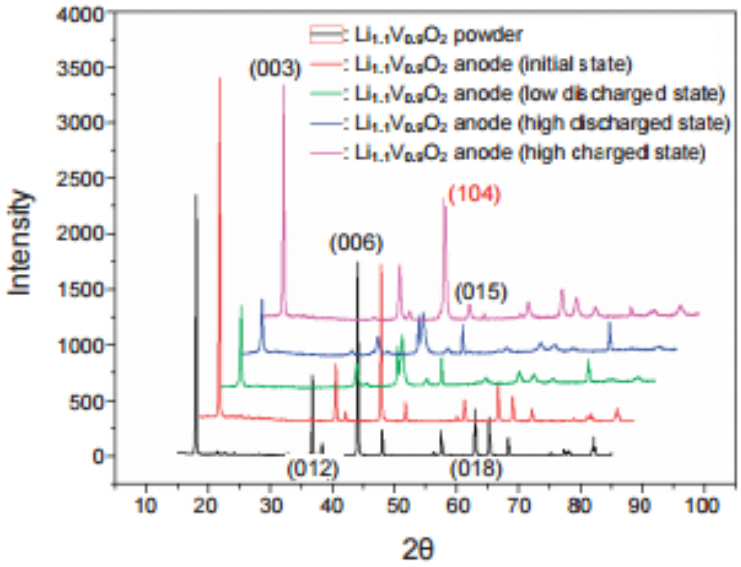

Figure 2.11: XRD patterns of the $Li_{1.1}V_{0.9}O_2$ anode before and after cycle test at 0.1C (charging) rate [36].

2.3.2 Morphological Properties

Scanning electron microscope (SEM) is an imaging technique employed in this experiment to study the morphology of LiV_3O_8 by scanning a fine beam of electrons across the material surface. Among the factors of the electrochemical performance of LiV_3O_8, particle size and shape and state of agglomeration will be discussed as they are the main studies from the SEM micrographs. An example of pristine LiV_3O_8 is shown in Figure 2.12 [15]. Also worth to note that the SEM micrographs are to be observed before and after cycling to observe the decomposition of materials in the electrode and hence to examine the relationship between cycling and resulting micrographs.

As reported previously, calcination temperature and chelating agent are important factors which affect morphology. In this section, Zheng et al. [37] reported that there is a close relationship between the cooperation among the different components in the electrode. As the amount of inactive material; polyvinylidene difluoride (PVDF)-to-acetylene black (AB) ratio increases, the rate capability increases

as the amount of AB essentially increases. The result is explained by the competition between the ion-blocking effect of PVDF binder and the electronic conducting effect of the AB additive. As reported, the SEM micrographs of $LiNi_{0.8}Co_{0.15}Al_{0.05}O_2$ composite electrodes have different amount of inactive materials at different composition.

At a low percentage of 2% PVDF and 1.2% AB, the electrode is shows as a stack of active material with an average size of spherical particle size measuring 6 μm (Figure 2.13). It is deduced that nanocarbon agglomerates are not homogenously dispersed in the electrode as they can easily flocculate as a result of their large surface area and high oil adsorption properties. To indicate a contrast, when the inactive material was increased to 8% PVDF and 4.8% AB, percolation of nanocarbon particulates is developed though not achieving complete homogeneity. Continuous electronic paths are developed within the electrode side to side when the conductive network is interconnected by particle to particle contact. At the highest point where there is 15% PVDF and 9% AB, the active material particles are seen immersed into the matrix of the PVDF/AB composite.

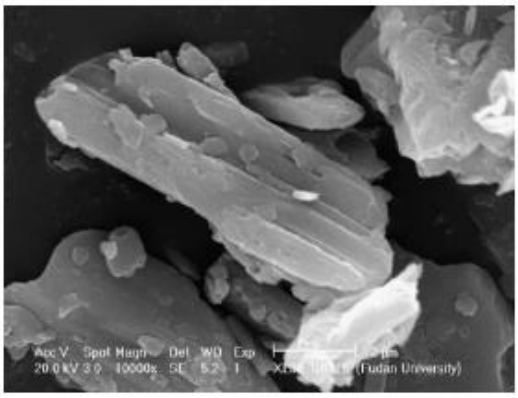

Figure 2.12: Scanning electron micrograph of the as-prepared LiV_3O_8 particles [15].

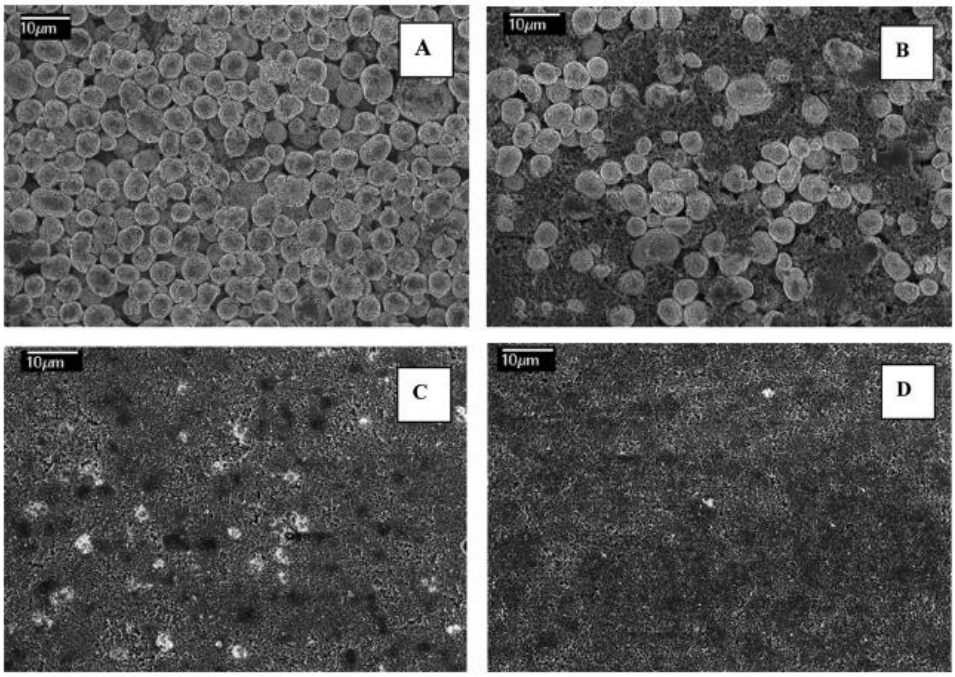

Figure 2.13: SEM images of the $LiNi_{0.8}Co_{0.15}Al_{0.05}O_2$ composite electrodes containing different amounts of inactive materials at a fixed PVDF/AB ratio of 5:3. (A: 2%PVDF + 1.2% AB. B: 8% PVDF + 4.8% AB. C: 15% PVDF + 9% AB. D: 20% PVDF + 12% AB) [37].

2.4 Electrochemical Properties of LiV_3O_8 in Batteries

2.4.1 Cyclic Voltammetry

In the studies of the electrochemical performance of LiV_3O_8 electrode, cyclic voltammetry (CV) is necessary to determine the stability of the redox processes based on quantitative measurement of the intercalation/de-intercalation of Li^+ will be reviewed to understand the entire process.

Electrochemical stability of water is the range of potential at a certain pH where water is thermodynamically stable. The fact that O_2 and H_2 is generated causes decomposition and this occurs to electrode materials outside the electrochemical stability range of water (Figure 2.14). Outside the electrochemical stability range of

water, the electrode reactant react with water, absorbing lithium with the concurrent generation of protons, causes a reduction in pH of water [38].

Therefore, it is important that the electrode materials avoid the evolution of O_2 and H_2 during the intercalation and de-intercalation processes respectively. The CV of the electrode in the saturated $LiNO_3$ solution obtained by Wang et al. [38] is shown (Figure 2.14). Two peaks with 1.8 V and -1.0 V are observed and they correspond to the generation of O_2 and H_2 respectively, indicating that the range of stable electrochemical window of water is about 2.8 V. According to Nerst's equation, this value is affected by pH [39].

$$E = E^0 - \left(\frac{RT}{nF}\right) lnQ \tag{2.5}$$

Where; E is the cell potential, E^0 is the standard cell potential, R is the universal gas constant T is the absolute temperature, n is the number moles of electrons transferred in the cell reaction, F is the Faraday constant and Q is the reaction quotient (depending on the structure of vanadate).

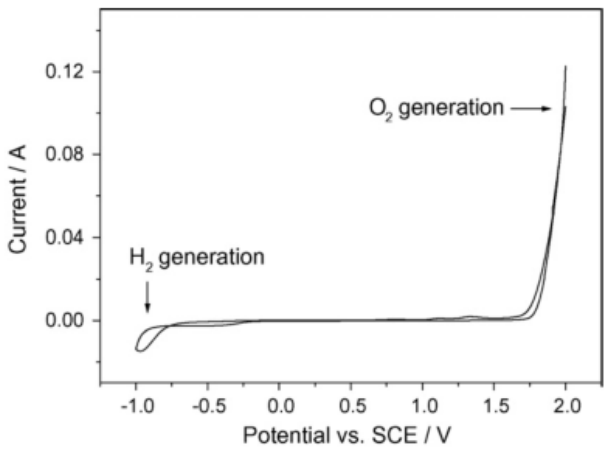

Figure 2.14: CV for nickel electrode in saturated $LiNO_3$ aqueous solution [38].

Also, the cyclic voltammogram of LiV_3O_8 used as anode in the saturated $LiNO_3$ solution with pH 6.2 using saturated calomel electrode as reference electrode is shown in Figure 2.15. As observed, the redox peaks at -0.19 and 0.098 V (vs SCE) corresponds to the intercalation and de-intercalation of lithium ions involving the movement of electrons can be represented in:

Eqs. (2.6) and (2.7):

Charge : $LiV_3O_8 + xLi^+ + xe^- \rightarrow Li_{1+x}V_3O_8$ (x < 1, at about −0.19 V) (2.6)

Discharge : $Li1_{+x}V_3O_8 \rightarrow LiV_3O_8 + xLi^+ + xe^-$ (x < 1, at about 0.098 V) (2.7)

From the study, it is evident that LiV_3O_8 can be used as electrode material in aqueous solution given that the observed redox potential is -0.0046V (vs SCE) which is higher that the hydrogen evolution potential at <-0.8V vs SCE.

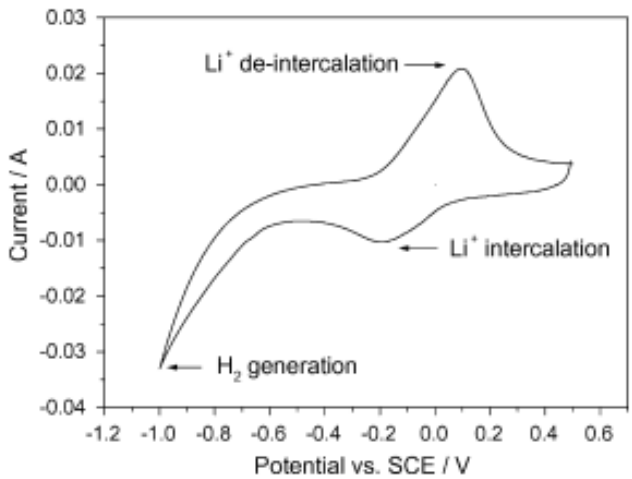

Figure 2.15: Cyclic voltammogram of LiV_3O_8 in saturated $LiNO_3$ aqueous electrolyte with scanning rate of 2 mV/s using SCE as reference electrode system [38].

When different scan rates are used with LiV_3O_8 anode immersed in 0.5M Li_2SO_4 aqueous electrolyte, still having consistent redox peaks between -0.6 and 0.2 V (vs SCE), indicating to the insertion and extraction of lithium ions into and from the anode (Figure 2.15) [41]. With the increase in scan rate, the peak current tends to be larger